Journal of
Materials Chemistry A

Accepted Manuscript

This article can be cited before page numbers have been issued, to do this please use: D. Wang, Y. Si, J. Li and Y. Fu, *J. Mater. Chem. A*, 2019, DOI: 10.1039/C9TA01273G.

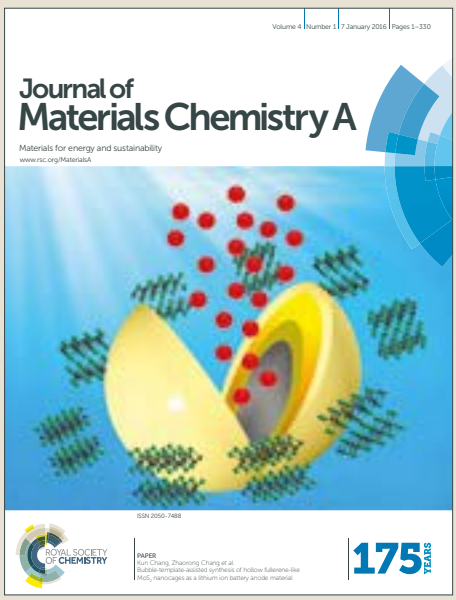

ROYAL SOCIETY OF CHEMISTRY

rsc.li/materials-a

View Article Online
DOI: 10.1039/C9TA01273G

ARTICLE

Tuning the Electrochemical Behavior of Organodisulfides in Rechargeable Lithium Batteries by N-Containing Heterocycles

Received 00th January 20xx,
Accepted 00th January 20xx

DOI: 10.1039/x0xx00000x

Dan-Yang Wang,[a] Yubing Si,*[b] Junjie Li,[c] and Yongzhu Fu*[a]

S-S bonds in organodisulfides can break then take Li^+ and e^- in the discharge of lithium batteries. They provide precise lithiation sites, therefore are valuable models for the study of redox reactions in lithium battery. To regulate their electrochemical behavior, we investigate three disulfides with different N-containing heterocycles including 2,2'-dipyridyl disulfide (2,2'-DpyDS), 4,4'-dipyridyl disulfide (4,4'-DpyDS), and 2,2'-dipyridyl disulfide-N,N'-dioxide (DpyDSDO). The three disulfides all show higher discharge voltage plateaus due to the electron-withdrawing groups: DPDS (2.20 V) < 2,2'-DpyDS (2.45 V) = 4,4'-DpyDS (2.45 V) < DpyDSDO (2.80 V). In particularly, 2,2'-DpyDS exhibits outstanding 500 cycles with 69% capacity retention. Our theoretical simulations show the lithium pyridine-2-thiolate, as the discharge product of 2,2'-DpyDS, forms compact clusters via N···Li···S bridges coordinated by lithium ions, which can help reduce its dissolution in liquid electrolyte, therefore increase cycle life. Liquid chromatography-mass spectrometry is demonstrated to be a powerful tool for the investigation of discharge/recharge products of soluble organodisulfides in rechargeable lithium batteries.

Introduction

Lithium-ion (Li-ion) batteries have dominated most energy storage markets ranging from portable electronics to electric vehicles.[1] Currently, transition metal oxides such as $LiCoO_2$ and its derivatives are being widely used as cathode materials.[2,3] However, their specific capacities are limited to be 140-250 mAh g^{-1} due to ion intercalation storage mechanism.[4] In addition, Co is not only expensive, but also toxic leading to safety hazard.[5] On the other hand, the economically abundant and structurally flexible organic compounds, containing free radical,[6] carbonyl,[7,8] and polysulfides[9,10], can potentially serve as great alternative cathode materials for lithium batteries. The most appealing aspect of these materials lies on the unique charge storage mechanism allowing multi-electron transfer per molecule, which is promising for building high capacity batteries. Organic electrode materials undergo conversion reactions in batteries, involving changes of structure and composition.[11] Their electrochemical behavior can be modulated by the functional groups attached to the active sites.[12-14] Therefore, understanding their structure/property relationships is valuable for developing new high-capacity electrode materials.

Organodisulfides containing S-S bonds have been demonstrated to be feasible electrode materials for rechargeable lithium batteries since the first research by Visco in 1988.[15] It was discovered that in the redox reactions of these materials, such as those happen in diphenyl disulfide (DPDS) and tetraethylthiuram disulfide, a single S-S bond breaks and re-forms involving $2Li^+$ and $2e^-$ per molecule.[16] Subsequently a number of polymeric organosulfides that have multiple S-S bonds have also been applied in lithium batteries.[17-19] These materials were studied to some extent, however not being thoroughly characterized due to limited characterization techniques applied. Recently, our groups made some efforts to expand the organosulfide electrode family. Dimethyl trisulfide,[20] diphenyl trisulfide,[21] thiuram polysulfides,[22] and diphenyl polysulfides[23,24] were studied as cathode materials, which showed unique property and performance in rechargeable lithium batteries. In particular, thiuram polysulfides showed very stable cycling performance, which is partially due to the N-containing functional groups attached to the sulfur active sites. The formed N^+ center in the heterocycle of discharge leads to charge transfer from Li_2S_4, Li_2S_2, and Li_2S, therefore retaining discharged products in the electrodes.[25] This study inspires more interest in understanding the effect of N-containing heterocycles on the electrochemical behavior of organosulfides in rechargeable lithium batteries.

In this work, we investigate dipyridyl disulfides in comparison with DPDS in lithium batteries. All these disulfides undergo the cleavage of disulfide bonds in the discharge (lithiation reaction) and re-formation of disulfide bonds in the recharge (de-lithiation reaction). DPDS can deliver a theoretical capacity of 245 mAh g^{-1},[26] however, it has slow reaction kinetics and severe

[a] College of Chemistry and Molecular Engineering, Zhengzhou University, Zhengzhou 450001, P. R. China. *E-mail: yfu@zzu.edu.cn
[b] Henan Provincial Key Laboratory of Nanocomposites and Applications, Institute of Nanostructured Functional Materials, Huanghe Science and Technology University, Zhengzhou 450006, P. R. China. *E-mail: yubingsi@infm.hhstu.edu.cn
[c] Research Technologies Indiana University, Indianapolis, IN 46202, U. S. A.
Electronic Supplementary Information (ESI) available: [details of any supplementary information available should be included here]. See DOI: 10.1039/x0xx00000x

View Article Online
DOI: 10.1039/C9TA01377C

capacity decay. In contrast, the three selected dipyridyl disulfides, *i.e.*, 2,2'-dipyridyl disulfide (2,2'-DpyDS), 4,4'-dipyridyl disulfide (4,4'-DpyDS), and 2,2'-dipyridyl disulfide-N,N'-dioxide (DpyDSDO), have N-containing heterocycles and similar theoretical capacities (Scheme 1). 2,2'-DpyDS and 4,4'-DpyDS have N atoms on the ortho and para positions, respectively, in the pyridyl ring. DpyDSDO has nitro groups on the ortho positions. Study on the structure-performance relationship will provide us with valuable insight on tuning their electrochemical behivior in lithium batteries, thus guide us to design more powerful organosulfides cathode materials.

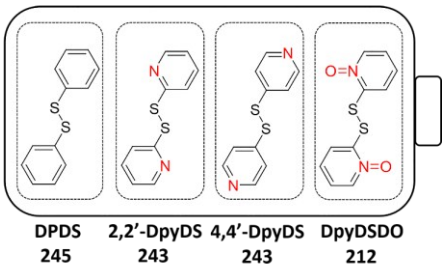

Scheme 1. Chemical structures of diphenyl disulfide (DPDS), 2,2'-dipyridyl disulfide (2,2'-DpyDS), 4,4'-dipyridyl disulfide (4,4'-DpyDS), and 2,2'-dipyridyl disulfide-N,N'-dioxide (DpyDSDO), the values are their theoretical specific capacities.

Experimental

Preparation of Carbon Nanotube Current Collector and Catholytes

160 mg multi-walled carbon nanotubes (MWCNTs, Nanostructure and Amorphous Materials, Inc.) were dispersed in a miscible solution of de-ionized water (500 mL) and isopropyl alcohol (20 mL) by ultra-sonication for 15 min, followed by vacuum filtration to render a free-standing MWCNT paper. The MWCNT paper was dried in an air-oven for 24 h at 100 °C before being peeled off and punched out into circular disks with 1.1 cm diameter (0.97 cm^2, 3-4 mg). The catholytes were prepared by dissolving 0.25 mmol (55 mg) 2,2'-DpyDS or 4,4'-DpyDS in 1 mL of 1.0 M lithium bis(trifluoromethanesulfonyl)imide (LiTFSI) in 1,3-dioxolane (DOL):1,2-dimethoxyethane (DME) =1:1 v/v with 1.0 wt.% $LiNO_3$ in an Argon-filled glove box. The catholyte concentration is 0.25 M. 1.0 M and 1.5 M 2,2'-DpyDS catholytes were also prepared and their battery performances were evaluated.

Cell Fabrication and Electrochemical Evaluation

Coin cells CR2032 were fabricated in the glove box. First, 2,2'-DpyDS or 4,4'-DpyDS catholyte (20 µL) was added into the MWCNT paper current collector. Then a Celgard 2400 separator was placed on the top of the MWCNT paper electrode followed by adding 20 µL electrolyte on the top of the separator. Finally, lithium metal anode was placed on the separator. The cell was crimped and taken out of the glove box for testing. This cell configuration has been demonstrated to be effective in evaluating soluble active material in lithium batteries.[27] DpyDSDO is insoluble in the electrolyte, therefore it was evaluated in sandwiched electrode configuration. A certain amount (~2 mg) of DpyDSDO was sandwiched in two pieces of MWCNT paper in the glove box. 30 µL electrolyte was added into the sandwiched electrode. The following procedure is same as described above.

Characterizations

X-ray diffraction (XRD) data were collected on a Rigaku Miniflex 600 XRD Instrument equipped with Cu Kα radiation. The samples were protected in the sample holder by Kapton tape. The scanning rate is 0.5° min^{-1}, and 2θ is between 20° and 80°. The XRD patterns of pristine 2,2'-DpyDS, DpyDSDO and electrodes after discharge and recharge were also collected for comparison. X-ray photoelectron spectroscopy (XPS) were analyzed with a 5000 VersaProbe II PS spectrometer with monochromatic Al Kα radiation. All samples were transferred without exposing in air. Cyclic voltammetry (CV) was performed on a BioLogic VSP potentiostat. The potential was swept from open circuit voltage to 2.0 V and then swept back to 3.0 V at a scanning rate of 0.05 mV s^{-1} for DpyDS, the potential window for the Li/DpyDSDO cell is 1.9-3.5 V. The Li/DpyDS cells were galvanostatically cycled at 2.0-3.0 V on a LAND battery cycler at different C rates (1C = 243 mA g^{-1}, based on the mass of DpyDS in the cells). The Li/DpyDSDO cell was galvanostatically cycled at 2.0-3.4 V at different C rates (1C = 212 mA g^{-1}, based on the mass of DpyDSDO in the cell). Liquid chromatography-mass spectrometry (LC-MS) was performed on an Agilent 6420 Triple Quad LC/MS equipment. The samples were dissolved in chromatographic methanol and 1 µL solution was tested and separated by C18 column (2.1 × 100 mm, 3.5 µm particle size, Agilent) under atmospheric pressure chemical ionization (APCI) positive mode.

Sample Preparation and LC-MS Measurements

The discharged and charged cathodes were immersed in 1 mL chromatographic methanol separately and the solution was fully shaken by hand. 10 µL of such solution was taken by a pipette and added to a LC-MS vial with 1 mL additional chromatographic methanol. The same gradient elution method was used for all samples in the LC-MS measurements. The solvent phase for the LC was from 20/80% to 80/20% CH_3OH/H_2O between 0-4 minutes, then it was 80/20% CH_3OH/H_2O between 4-25 minutes. The injection volume was 1 µL and the solvent phase velocity was 0.2 mL min^{-1}.

For the solubility test, the 2,2'-DpyDS and 4,4'-DpyDS electrodes after discharge were immersed in 1 mL electrolyte separately and the solution was fully shaken by hand. 10 µL of such solution was taken by a pipette and added to a LC-MS vial with 1 mL additional chromatographic methanol. The following procedures are same as above.

Theoretical Simulations

The simulations were performed using the Gaussian 09 computational chemistry package.[28] Solvation model based on density (SMD) was employed to take account of the solvation effect,[29] and the static dielectric constant of DME was set to ϵ = 7.07 at 298.15K.[30] The charge/discharge compounds were

optimized with density functional theory (DFT) at PBE0/cc-pVTZ level along with vibrational frequency analysis confirming the optimized geometries to be true local minima. In order to eliminate the difference of the cycling stability of 2,2'-DpyDS and 4,4'-DpyDS. Born Oppenheimer Molecular Dynamics (BOMD) simulations at B3LYP/6-31G(d) level of theory were performed for two systems, each containing four optimized 2,2'-DpyDS or 4,4'-DpyDS. Initial kinetic energies of the BOMD simulations were set to zero and time steps were fixed to 0.5 fs.

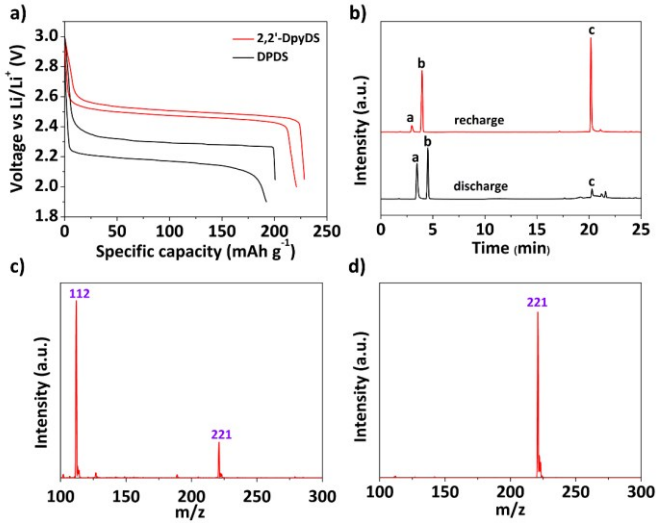

Figure 1. a) Voltage-capacity profile of Li/2,2'-DpyDS and Li/DPDS cells in the first cycle at C/10 rate; b) Total ion chromatograms of 2,2'-DpyDS electrodes after discharge and recharge: a, b, and c represent the protonated 2-pyridinethiol, LiTFSI, and 2,2'-DpyDS, respectively; Mass spectra of a peak c) and c peak d).

Results and discussion

Cycled Products of 2,2'-DpyDS Characterized by LC-MS, XRD, and XPS

Here we take the first research on 2,2'-DpyDS and DPDS. Their first discharge/recharge voltage profiles are shown in Fig. 1a. 2,2'-DpyDS has ortho-N groups and it can be seen that the Li/2,2'-DPyDS cell exhibits a discharge voltage plateau at 2.45 V, more than 10% higher than that (2.20 V) of DPDS. Furthermore, the voltage hysteresis between discharge and recharge of the Li/2,2'-DPyDS cell is only 0.04 V which is significantly smaller than that (0.10 V) of the Li/DPDS cell, indicating the former cell has better energy efficiency and faster reaction kinetics. The Li/2,2'-DPyDS cell delivers a discharge specific capacity of 228 mAh g^{-1} (*i.e.*, 94% of the theoretical capacity of 2,2'-DPyDS), while the discharge specific capacity of the Li/DPDS cell is 192 mAh g^{-1} (*i.e.*, 78% of the theoretical capacity of DPDS).

LC-MS was used to identify the discharge and recharge products of 2,2'-DpyDS. Fig. 1b shows the total ion chromatograms (TIC). The discharge TIC shows three peaks at retention times of 3.9, 4.2 and 20.1 min labeled as **a**, **b**, and **c**, respectively. The m/z of **a** peak is 112 (Fig. 1c), corresponding to the protonated 2-pyridinethiol, which is the form of lithium pyridine-2-thiolate, *i.e.*, discharge product of 2,2'-DpyDS, in the LC-MS analysis under APCI positive mode. The lithium salt LiTFSI in the electrolyte leads to **b** peak, the corresponding mass spectrum is attached in Fig. S1. The m/z of the negligible **c** peak is same as that of 2,2'-DpyDS (Fig. 1d and S1), suggesting **a** negligible amount of 2,2'-DpyDS not being fully reduced. The recharge plot also shows three peaks with similar retention times. Apparently, 2,2'-DpyDS is recovered as indicated by the strong **c** peak, while there is still a very small amount of discharge product. The LC-MS can clearly identify the cycled products of 2,2'-DpyDS in lithium cells with high accuracy.

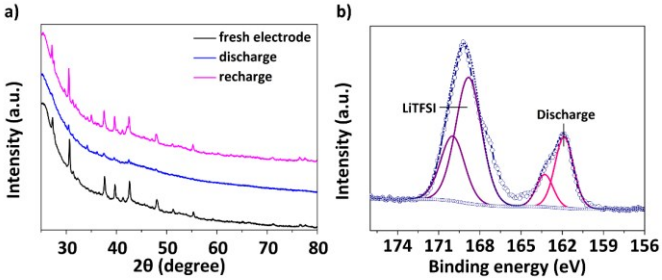

Figure 2. a) X-ray diffractograms of the 2,2'-DpyDS electrode before and after discharge and recharge; b) XPS spectrum of sulfur 2p of the 2,2'-DpyDS electrode after discharge.

XRD of the 2,2'-DpyDS electrode was measured after discharge and recharge (Fig. 2a). The peak of CNTs at 26.4° is blurred due to the coverage of Kapton film. Characteristic peaks of 2,2'-DpyDS at 30.4°, 37.4°, 39.6°, 42.4°, 48.0°, and 55.3° are observed in the freshly-made electrode. After discharge, these peaks are nearly all gone indicating conversion of 2,2'-DpyDS. After recharge, characteristic peaks of the starting material reappear representing the reformation of 2,2'-DpyDS. The XRD of commercial 2,2'-DpyDS is shown in Fig. S2, which is different from that of the freshly-made electrode due to the change of the crystalline phases formed from the electrolyte solution. To identify the discharge product of the 2,2'-DpyDS, XPS was also performed (Fig. 2b). The doublet peaks of S $2p_{3/2}$ and S $2p_{1/2}$ centered at 162.0 and 163.2 eV are attributed to the discharge product of 2,2'-DpyDS. These are lower than the S 2p binding energies of the starting material (Fig. S3) indicating sulfur is in the reduced state. The results obtained from the conventional XRD and XPS techniques support the reversibility of the redox reaction of 2,2'-DpyDS in lithium cells.

Cycled Products of 4,4'-DpyDS and DpyDSDO Characterized by LC-MS, XRD, and XPS

The pyridyl group with ortho-N can increase discharge voltage plateau and utilization of organodisulfides in lithium batteries. Next, we study the effect of nitrogen on the para position (para-N) and nitro group (ortho-NO) on the electrochemical behavior of disulfides. Fig. 3a presents the voltage profiles of Li/4,4'-DpyDS and Li/DpyDSDO cells. The Li/4,4'-DpyDS cell shows a similar discharge plateau at 2.45 V as that of the Li/2,2'-DpyDS cell and the Li/DpyDSDO cell shows a high discharge voltage plateau at about 2.80 V. The initial discharge specific capacities of 4,4'-DpyDS and DpyDSDO are 209 and 159 mAh g^{-1},

View Article Online
DOI: 10.1039/C9TA01273G

corresponding to 86 and 75% of their theoretical capacities, respectively. The high voltage hysteresis of the Li/ DpyDSDO cell could be due to the sandwiched electrode having high ohmic resistance.

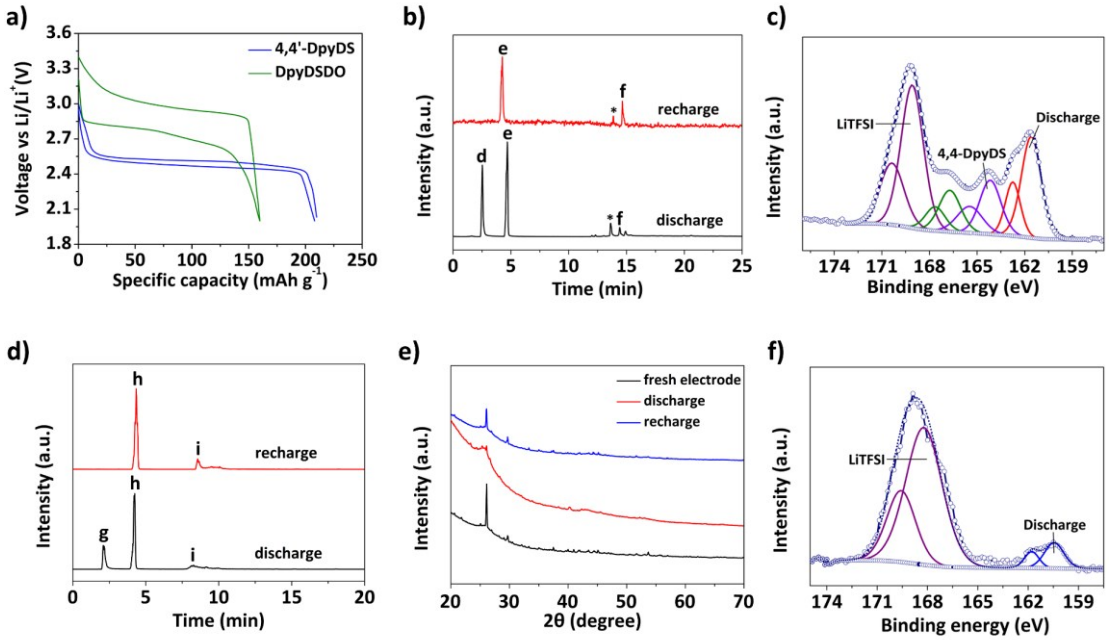

Figure 3. a) Voltage-capacity profile of Li/4,4'-DpyDS and Li/DpyDSDO cells in the first cycle at C/10 rate; b) TICs of the 4,4'-DpyDS electrode after discharge and recharge: d, e, f, and * represent the protonated 4-pyridinethiol, lithium salt, 4,4'-DpyDS, and impurity, respectively; c) XPS spectrum of sulfur 2p of the 4,4'-DpyDS electrode after discharge; d) TICs of the DpyDSDO electrode after discharge and recharge: g, h, and i represent protonated 2-pyridinethiol N-oxide, lithium salt, and DpyDSDO, respectively; e) X-ray diffractograms of Li/DpyDSDO cathode at different stages of cycling; e) XPS spectrum of sulfur 2p of the 4,4'-DpyDS electrode after discharge.

LC-MS was performed on the 4,4'-DpyDS and DpyDSDO electrodes after discharge and recharge. The TIC of 4,4'-DpyDS after discharge clearly displays the appearance of **d** peak of the protonated 4-pyridinethiol at 2.6 min and weakening of **f** peak of 4,4'-DpyDS in Fig. 3b. The corresponding mass spectra are shown in Fig. S4. In the recharge, 4,4'-DpyDS is recovered. XPS of the discharge electrode of 4,4'-DpyDS was also tested. The S $2p_{3/2}$ and S $2p_{1/2}$ doublet peaks located at 161.6 and 162.8 eV, respectively, are assigned to the discharge product. There is some unreacted raw material with the S $2p_{3/2}$ and S $2p_{1/2}$ peaks located at 164.0 and 165.0 eV, respectively, in the sample (Fig. 3c and S5). The discharged and recharged electrodes of 4,4'-DpyDS do not show any crystalline peaks in XRD, therefore they are not given.

The TIC of DpyDSDO after discharge in Fig. 3d combined with the mass spectra results in Fig. S6 show the emergence of **g** peak of the protonated 2-pyridinethiol *N*-oxide and weakening of **i** peak of DpyDSDO. Peaks of **e** and **h** are due to LiTFSI. Therefore, these LC-MS data substantiate the substances after discharge and recharge of 4,4'-DpyDS and DpyDSDO. The XRD patterns of DpyDSDO are shown in Fig. 3e. The fresh prepared electrode shows two major peaks at 25.9° and 29.6°, which are consistent with those of the pristine DpyDSDO (Fig. S7). Upon discharge, these characteristic peaks disappear. After recharged, these peaks are recovered. The XPS analysis of the discharged product of DpyDSDO leads to S 2 $p_{3/2}$ and S 2 $p_{1/2}$ doublet peaks at 160.6 and 161.8 eV, respectively (Fig. 3f), which are lower than those of DpyDSDO (Fig. S8). It can be seen that the XPS spectrum of the DpyDSDO electrode after discharge is quite clean, meaning the reduction reaction is complete. However, the discharge of 4,4'-DpyDS is incomplete resulting in residual starting material. The XPS results are consistent with the LC-MS analysis.

In order to further understand the redox processes of the three compounds in lithium batteries, first-principles DFT calculations were performed. The equilibrium geometries of 2,2'-DpyDS, 4,4'-DpyDS, and DpyDSDO and the corresponding discharge stable configurations are shown in Fig. 4a. Since the discharge voltages of all three compounds are increased, the connection between lithium and electron-withdrawing nitrogen or nitro groups has been queried after discharge. While the calculation results demonstrate the lithium atoms are still connected with sulfur atoms after discharge. From the lowest unoccupied molecular orbital (LUMO) and highest occupied molecular orbital (HOMO) energies of three geometries (Fig. 4b), apparently, the compound containing the strongest electron-withdrawing nitro group has the lowest LUMO of -1.60 eV. The LUMO levels of three geometries and discharge voltage plateaus are reversibly related meaning DpyDSDO has the highest discharge voltage plateau among these three compounds, which are all attributed to the introduction of strong electron-withdrawing nitro group.[31]

Cycling Performance of Li/DPDS, Li/2,2'-DpyDS, Li/4,4'-DpyDS, and Li/DpyDSDO cells

All four cells' cycling performances are shown in Fig. 4c. 2,2'-DpyDS presents an initial discharge capacity of 237 mAh g^{-1}

andthe capacity retention rate is 69% after 500 cycles. The Coulombic efficiency (CE) is above 99.6% except the first ten

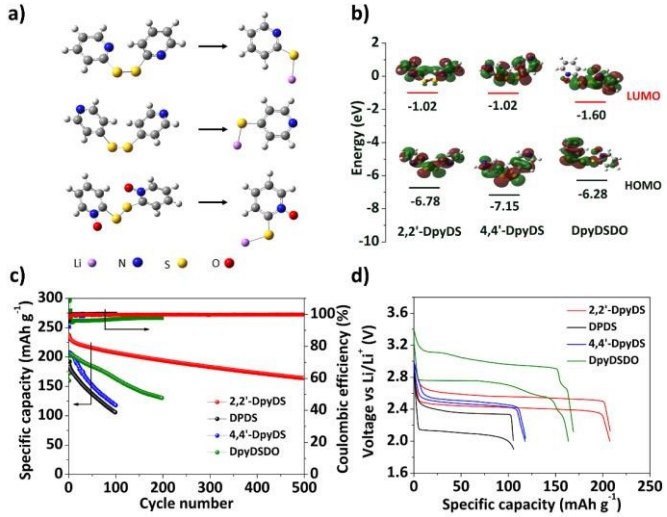

Figure 4. a) Equilibrium structures of the discharge process of 2,2'-DpyDS, 4,4'-DpyDS, and DpyDSDO; b) electron density of the lowest unoccupied molecular orbital (LUMO) and highest occupied molecular orbital (HOMO) orbitals of three compounds, as calculated at the PBE0/SMD/cc-pVTZ level; c) cycling performance of Li/2,2'-DpyDS, Li/DPDS, Li/4,4'-DpyDS and Li/DpyDSDO cells at C/2 rate; d) the voltage-capacity profiles of these cells in the 100th cycles.

cycles. In contrast, DPDS only displays an initial discharge capacity of 193 mAh g^{-1} and the capacity retention is only 54% after 100 cycles. The voltage profiles of selected cycles are shown in Fig. S9. The pyridyl group with ortho-N, in comparison with the phenyl group, can increase the discharge voltage, energy efficiency, and cycling stability of organodisulfides in rechargeable lithium batteries. However, 4,4'-DpyDS delivers an initial specific capacity of 208 mAh g^{-1}, while its capacity retention drops to 57% after 100 cycles, which is just comparable with that of DPDS. Its initial CE is 92.2%, and it increases to be >99.3% afterwards. DpyDSDO presents an initial specific capacity of 160 mAh g^{-1} and retains 82% of initial capacity after 200 cycles. The voltage-capacity profiles of these cells in the 100th cycle are shown in Fig. 4d. The Li/DPDS cell shows significant capacity decay and rise in overpotential. All the other three cells do not exhibit obvious overpotential increase or voltage profile change. The only difference lies on the distinguished capacity retention of the Li/2,2'-DpyDS cell after 100 cycles. Impedance data of the four cells before cycling are shown in Fig. S10. It can be seen that the charge transfer resistance of the Li/2,2'-DpyDS cell is much smaller than those of the other three cells, indicating its good electrochemical behavior.

The Li/2,2'-DpyDS cell shows outstanding performance in terms of cycling stability, which is also reflected by the overlapping CVs over 11 cycles, as shown in Fig. S11. It also shows good rate capability (Fig. S12). Discharge capacities of 218, 198, 192, 188, and 170 mAh g^{-1} have been obtained at C/10, C/2, 1C, 2C, and 5C, respectively. It also shows that the decline of capacity is extremely slow except at 5C. After 70 cycles, the discharge capacity is recovered to 191 mAh g^{-1} when the rate returns to C/10. The ohmic overpotential increases gradually as the C-rate increases, as shown in the voltage profiles at different rates. The CV and rate capability of the Li/4,4'-DpyDS and Li/DpyDSDO cells are also examined (Fig. S13). A cathodic peak at 2.39 V and an anodic peak at 2.60 V are observed from the CV curve of the Li/4,4'-DpyDS cell, while the Li/DpyDSDO cell has two cathodic peaks at 2.80 and 2.45 V and three anodic peaks at 2.52, 3.01 and 3.27 V. Unfortunately, the rate performance of both cells presents poorer recovery than the Li/2,2'-DpyDS cell.

To achieve high specific energy, high mass loading of active material with minimal electrolyte (*i.e.*, low electrolyte to active material ratio) is needed (Fig. S14).[32] Owing to the high discharge voltage of 2.45 V, 2,2'-DpyDS has a theoretical specific energy of 585 Wh kg^{-1} which is higher than that of the DPDS. When 1.0 M and 1.5 M 2,2'-DpyDS catholytes are used, the Li/2,2'-DpyDS cells deliver initial specific energies of 436 and 392 Wh kg^{-1} (based on the masses of 2,2'-DpyDS), respectively, and good cycling stability. The 2,2'-DpyDS mass loadings are 4.4 and 6.6 mg cm^{-2}, and the electrolyte/2,2'-DpyDS ratios are as low as 4.5 and 3.0 mL g^{-1}, respectively.

Understanding the Cycling Performance Degradation of 4,4'-DpyDS and 2,2'-DpyDS

The cycling stability of the Li/4,4'-DpyDS cell is much worse than that of the Li/2,2'-DpyDS cell. To find out the reason, LC-MS was used to quantitatively compare the remaining discharged products of 4,4'-DpyDS in the electrodes after the 1st and 100th discharges, as shown in Fig. 5a. The intensity of **d** peak decreases heavily after 100 cycles, showing loss of active material. As a result, the achievable capacity is significantly reduced. Secondly, we quantitatively compare the remaining discharged products of 2,2'-DpyDS and 4,4'-DpyDS in the electrodes after discharge (Fig. 5b). We assume the lithium salt contents in two electrodes are same, which are normalized to be 100. The dissolved products of the 2,2'-DpyDS and 4,4'-DpyDS electrodes after discharge are 38 and 59, respectively as

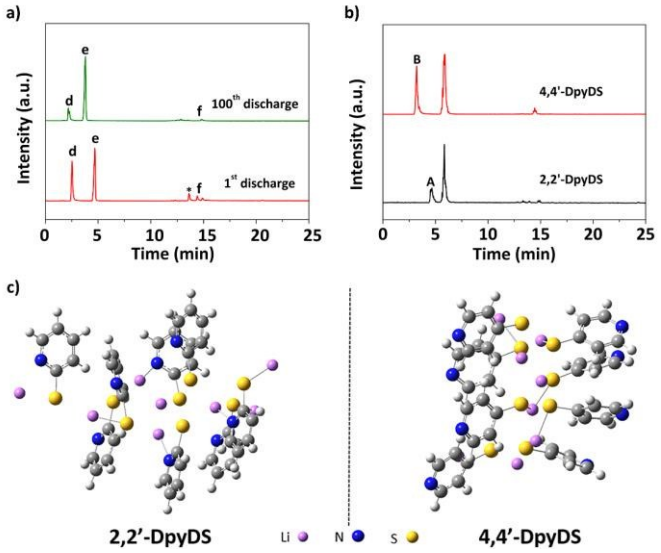

Figure 5. a) Ion chromatogram comparison of the 4,4'-DpyDS electrode after the 1st and 100th discharges; b) TIC of the 2,2'-DpyDS and 4,4'-DpyDS

electrodes after discharge; c) cluster structures of the discharged products of 2,2′-DpyDS and 4,4′-DpyDS.

Table 1. The normalized contents of soluble discharge products of 2,2′-DpyDS and 4,4′-DpyDS and Li salt in electrolyte.

	Discharge product	Li salt content
2,2′-DpyDS	38 (A)	100
4,4′-DpyDS	59 (B)	100

shown in Table 1. The soluble discharged product of 2,2′-DpyDS in the electrolyte is much less than that of 4,4′-DpyDS, indicating more discharged product of 2,2′-DpyDS is insoluble remaining in the electrode.

2,2′-DpyDS and 4,4′-DpyDS show clear difference in the cycling stability, which has been proved to be the result of solubility difference between the different discharged products as the starting materials are both quite soluble in liquid electrolyte. We use simulation to help clarify the difference. Stable configurations of the discharged products of 2′2-DpyDS and 4,4′-DpyDS are shown in Fig. 5c. It can be seen that the N, Li, and S atoms in lithium pyridine-2-thiolate are gathered to form a tight cluster structure via N···Li···S bridges.[33-35] In contrast, N atoms are distant away from Li and S atoms in lithium pyridine-4-thiolate. The S atom carries negative charge and N has a lone pair of electrons, therefore Li cations are attracted by N and S atoms via electrostatic forces. The ortho-N allows close interactions among them, whereas the para-N cannot. That's why the cycling performance of 2,2′-DpyDS is the most stable. The configuration of lithium pyridine-4-thiolate is too loose to suppress its dissolution in electrolyte because of S is too far from the para N atom. The selected snapshots along the BOMD trajectories show the evolution of configurations during discharge in Fig. S15 and S16.

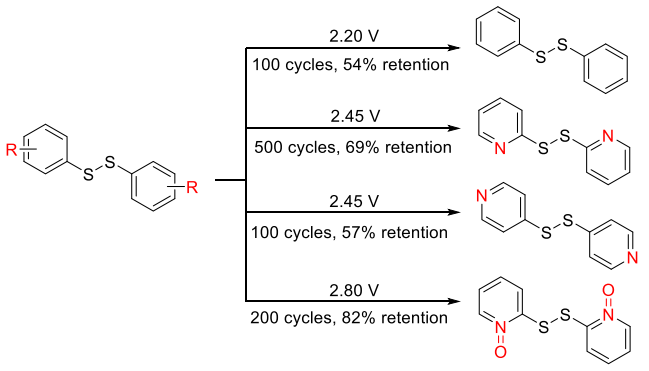

Scheme 2. Electrochemical behavior summary of DPDS, 2,2′-DpyDS, 4,4′-DpyDS, and DpyDSDO.

Conclusions

In conclusion, we have demonstrated the efficacy of using N-containing heterocycles to tune the electrochemical properties of organodisulfides as cathode materials in rechargeable lithium batteries. The discharge voltages and cycling retention rates of the four organodisulfides are summarized in Scheme 2. Detailed characterizations show that the discharge plateaus of disulfides can reach 2.45 V and 2.80 V when electron-withdrawing nitrogen atom and nitro groups are attached, respectively. The 2,2′-DPyDS with ortho-N exhibits long cycle life of 500 cycles, high Coulombic efficiency (over 99.6%), and 69% capacity retention. Its outstanding cycling performance is attributed to the tight clusters by N···Li···S bridges coordinated by lithium ions leading to low solubility of the discharged product of 2,2′-DPyDS. LC-MS was employed to identify the discharged and recharged products of soluble active materials and provide quantitative comparison, which can be a useful technique besides conventional XRD and XPS. This study reveals the redox reactions and correlates the structure-performance relationship of these organodisufides and the feasibility of regulating electrochemical behavior by structural adjustment in lithium batteries. Although disulfides have low specific capacities, strategies can be developed to introduce additional sulfur into the molecular structures to increase their capacities such as the method for the synthesis of diphenyl trisulfide.[21]

Conflicts of interest

There are no conflicts to declare.

Acknowledgements

YF acknowledges the startup support from Zhengzhou University and support from the Recruitment Program of Global Youth Experts in China.

Notes and references

1 M. Armand, J. M. Tarascon, *Nature*, 2008, **451**, 652-657.
2 J. B. Goodenough, K. S. Park, *J. Am. Chem. Soc.*, 2013, **135**, 1167-1176.
3 A. Manthiram, *J. Phys. Chem. Lett.*, 2011, **2**, 176-184.
4 J. B. Goodenough, Y. Kim, *Chem. Mater.*, 2010, **22**, 587-603.
5 L. O. Simonsen, H. Harbak, P. Bennekou, *Sci. Total Environ.*, 2012, **432**, 210-215.
6 W. Guo, Y. X. Yin, S. Xin, Y. G. Guo, L. J. Wan, *Energy & Environ. Sci.*, 2012, **5**, 5221-5225.
7 Z. Song, H. Zhan, Y. Zhou, *Angew. Chem. Int. Ed.*, 2010, **49**, 8444-8448.
8 Q. Zhao, Z. Zhu, J. Chen, *Adv. Mater.*, 2017, **29**, 1607007.
9 W. J. Chung, J. J. Griebel, E. T. Kim, H. Yoon, A. G. Simmonds, H. J. Ji, P. T. Dirlam, R. S. Glass, J. J. Wie, N. A. Nguyen, B. W. Guralnick, J. Park, A. Somogyi, P. Theato, M. E. Mackay, Y. E. Sung, K. Char, J. Pyun, *Nat. Chem.*, 2013, **5**, 518-524.
10 J. Liu, M. Wang, N. Xu, T. Qian, C. Yan, *Energy Storage Mater.*, 2018, **15**, 53-64.
11 Y. Liang, Z. Tao, J. Chen, *Adv. Energy Mater.*, 2012, **2**, 742-769.
12 S. Muench, A. Wild, C. Friebe, B. Haupler, T. Janoschka, U. S. Schubert, *Chem. Rev.*, 2016, **116**, 9438-9484.
13 Z. Guo, Y. Ma, X. Dong, J. Huang, Y. Wang, Y. Xia, *Angew. Chem. Int. Ed.*, 2018, **57**, 11737-11741.
14 M. Walter, K. V. Kravchyk, C. Bofer, R. Widmer, M. V. Kovalenko, *Adv. Mater.*, 2018, **30**, 1705644.
15 S. J. Visco, L. C. DeJonghe, *J. Electrochem. Soc.*, 1988, **135**, 2905-2909.
16 M. L. Liu, S. J. Visco, L. C. DeJonghe, *J. Electrochem. Soc.*, 1989, **136**, 2570-2575.
17 M. Liu, S. J. Visco, L. C. D. Jonghe, *J. Electrochem. Soc.*, 1991, **138**, 1891-1895.

View Article Online
DOI: 10.1039/C9TA01273G

18 H. Kim, J. Lee, H. Ahn, O. Kim, M. J. Park, *Nat. Commun.*, 2015, **6**, 7278.
19 M. B. Preefer, B. Oschmann, C. J. Hawker, R. Seshadri, F. Wudl, *Angew. Chem. Int. Ed.*, 2017, **56**, 15118-15122.
20 M. Wu, Y. Cui, A. Bhargav, Y. Losovyj, A. Siegel, M. Agarwal, Y. Ma, Y. Fu, *Angew. Chem. Int. Ed.*, 2016, **55**, 10027-10031.
21 M. Wu, A. Bhargav, Y. Cui, A. Siegel, M. Agarwal, Y. Ma, Y. Fu, *ACS Energy Lett.*, 2016, **1**, 1221-1226.
22 A. Bhargav, Y. Ma, K. Shashikala, Y. Cui, Y. Losovyj, Y. Fu, *J. Mater. Chem. A*, 2017, **5**, 25005-25013.
23 A. Bhargav, M. E. Bell, J. Karty, Y. Cui, Y. Fu, *ACS Appl. Mater. Inter.*, 2018, **10**, 21084-21090.
24 Y. Ma, *Energy & Environ. Mater.*, 2018, **1**, 148-173.
25 Y. Tang, B. L. Allen, D. R. Kauffman, A. Star, *J. Am. Chem. Soc.*, 2009, **131**, 13200-13201.
26 A. Bhargav, S. V. Patil, Y. Fu, *Sustainable Energy & Fuels*, 2017, **1**, 1007-1012.
27 Y. Fu, Y. S. Su, A. Manthiram, *Angew. Chem. Int. Ed.,* 2013, **52**, 6930-6935.
28 M. J. Frisch, G. W. Trucks, H. B. Schlegel, G. E. Scuseria, M. A. Robb, J. R. Cheeseman, G. Scalmani, B. M. V. Barone, G. A. Petersson, H. Nakatsuji, et al., Gaussian 09, Revision D.01, Gaussian, Inc.: Wallingford, CT, 2010.
29 V. M. Aleksandr, J. C. Christopher, G. T. Donald, J. Phys. Chem. B, 2009, **113**, 6378-6396.
30 Y. Cui, J. D. Ackerson, Y. Ma, A. Bhargav, J. A. Karty, W. Guo, L. Zhu, Y. Fu, *Adv. Funct. Mater.*, 2018, **28**, 1801791.
31 P. Peljo, H. H. Girault, *Energy & Environ. Sci.*, 2018, **11**, 2306-2309.
32 M. Hagen, D. Hanselmann, K. Ahlbrecht, R. Maça, D. Gerber, J. Tübke, *Advanced Energy Materials* 2015, **16**, 1401986.
33 J. C. Ye, J. J. Chen, R. M. Yuan, D. R. Deng, M. S. Zheng, L. Cronin, Q. F. Dong, *J. Am. Chem. Soc.*, 2018, **140**, 3134-3138.
34 W. Fan, N. W. Li, X. Zhang, S. Zhao, R. Cao, Y. Yin, Y. Xing, J. Wang, Y. G. Guo, C. Li, *Adv. Sci.*, 2018, **5**, 1800559.
35 J. H. Zeng, Y. F. Wang, S. Q. Gou, L. P. Zhang, Y. Chen, J. X. Jiang, F. Shi, *ACS Appl. Mater. Interfaces*, 2017, **9**, 34783-34792.

View Article Online
DOI: 10.1039/C9TA01273G

TOC entry

N-containing heterocycles can tune the electrochemical properties of organodisulfides in lithium batteries. 2,2'-Dipyridyl disulfide exhibits outstanding cycling stability.